

Stability Analysis of Grid Forming Converter Using 3-by-3 Admittance Measurements

Ali Aljumah, *Student Member, IEEE*, Zhixin Miao, *Senior Member, IEEE*, Lingling Fan, *Senior Member, IEEE*

Abstract—The objective of this paper is to conduct stability analysis on a grid forming voltage source converter (VSC). The effects of the dc-link control and the power droop parameters are investigated. Stability analysis is based on a 3×3 admittance model defining the current and voltage relationship viewed from dc and ac ports. The model is identified from experiment measurement data. The study shows that increasing the dc-link controller gain or the real power droop coefficient within suitable limits can enhance the dc-side stability of the VSC system. The analysis results have been verified by the electromagnetic transient (EMT) simulation results.

Index Terms—Stability analysis; grid forming converter; admittance model; system identification

I. INTRODUCTION

The penetration of inverter-based resources (IBRs) into power grids continues to rise, posing the potential of operating completely inverter-based power systems in different places around the world [1]. In the United States, as of 2020, around 20% of electricity is generated from renewable energy sources [2]. Most of this energy is from photo-voltaic and wind power systems [2], which are integrated to the grid using the VSCs. This increasing penetration has been causing variety of operation issues to power systems. Real-world events associated with IBRs have been reported worldwide, including subsynchronous resonance (SSR) events observed in Texas and west China [3], [4], solar PV tripping events in California [5].

An important factor that affects power systems' stability due to IBR integration is how inverters are controlled. Most of the current operating VSCs are controlled using the grid following method, where synchronization to the grid is achieved using a phase-locked-loop (PLL) [6]. With the decreasing number of synchronous generator-based resources, grid forming converters that can provide regulation on frequency and voltage are desired.

In the literature, research has been conducted to investigate the effects of grid forming control on system stability. For example, in [7], a comparative study between the grid following and grid forming control methods based on large signal stability was conducted. In [8], small signal stability based comparison between single loop and multi loop droop for grid forming control was performed and it was shown that the single loop droop control has a better effect on the VSC system's stability enhancement. Another study was performed in [9], where the weak grid operation of grid following and two grid forming converters were investigated and the advantage of the grid forming converter on weak grid stability is demonstrated.

The aforementioned studies focus on the ac network stability. In this paper, we examine the effect of grid forming control on dc network stability. The study relies on a 3×3 admittance model of the converter obtained through measurements [10], [11]. This modeling method shows the relation between dc-side voltage and current and ac-side voltage and current in dq -frame. In the authors' prior work [11], it was shown how the 3×3 admittance model can be developed based on transient response data and eigensystem realization algorithm (ERA), which converts time-domain data into s -domain expressions.

The current paper will use the measured 3×3 admittance model to investigate dc network stability for a grid forming converter integration system. The analysis takes into consideration of the effect of dc-link control and power droop parameters. Eigenvalue analysis based on the 3×3 admittance model is conducted. Furthermore, open-loop analysis based on the single-input single-output (SISO) system viewed from the dc side is also conducted. The analysis results are all validated by time-domain simulation results from the EMT test bed built in MATLAB/SimPowerSystems.

The remaining sections are organized as follows. Section II describes the study system and the control structure. In section III, the admittance measurement procedure and how to conduct stability analysis using this admittance are briefly explained. Analysis and validation are then presented in Section IV. Finally, the paper is concluded in Section V.

II. SYSTEM AND CONTROL STRUCTURES

A. Study System

Fig. 1 shows the test bed with a grid forming VSC as the major component interconnecting the dc network and the ac network. The dc voltage source is connected to the VSC through a series resistor (R_{dc}) and a shunt capacitor (C_{dc}). The VSC is connected to the grid through an RL filter and a line impedance ($Z_{Line} = R_g + jX_{L_g}$). Dc and ac networks are noted for the admittance modeling elaboration.

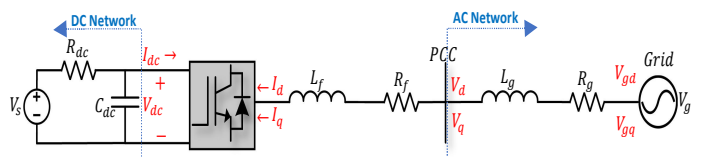


Fig. 1: Study system.

B. VSC Control Structure

Fig. 2 presents the block diagram of the control structure. In the grid forming control scheme, frequency command is generated via power measurement through a power-frequency droop control loop. Furthermore, the power command is generated through the dc-link voltage control [12]. If the dc-link voltage is less than its command, the power command will be reduced.

Besides the dc-link voltage/power/frequency control, there are two cascaded control loops: the inner current control loop and the outer control for ac voltage (V_{PCC}) regulation. The voltage command is generated by a var-volt droop. The q-axis voltage command is fixed at 0 to allow the d-axis voltage representing the ac voltage magnitude. The parameters of the test bed are shown in Table I.

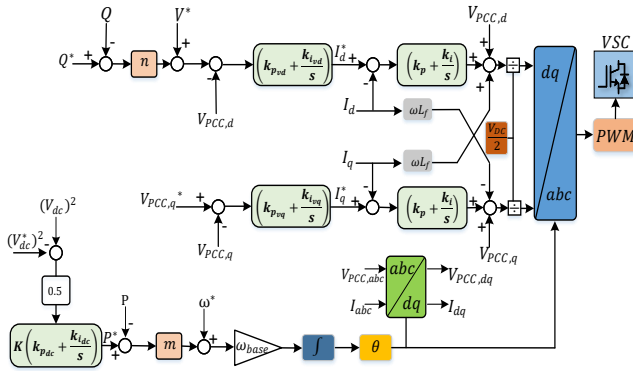


Fig. 2: Grid forming control.

TABLE I: System parameters.

Power Base	400 KVA	X_{L_f}	0.15 pu
Power level	0.925 pu	R_f	$0.1 * X_{L_f}$
AC Side Voltage	260 V	X_{L_g}	0.5 pu
dc-link voltage	500 V	R_g	$0.1 * X_{L_g}$
Inner loop k_p, k_i	0.3, 5	R_{dc}	0.64 pu
Outer loop k_{pvd}, k_{ivd}	1, 400	$X_{C_{dc}}$	0.0786 pu
Outer loop k_{pvq}, k_{ivq}	1, 10	m	0.2
dc control k_{pdc}, k_{idc}	0.5, 50	n	0.1

III. MODELING AND MEASUREMENT OF THE 3×3 ADMITTANCE

1) *Modeling*: The principle of the 3×3 admittance is to model the VSC independently from its dc and ac networks [10]. After that, this model can be aggregated to include ac, dc or both sides networks for various studies such as stability analysis. Equation (1) shows the admittance model.

$$\begin{bmatrix} \hat{I}_{dc}(s) \\ \hat{I}_d(s) \\ \hat{I}_q(s) \end{bmatrix} = \underbrace{\begin{bmatrix} Y_{ss}(s) & Y_{sd}(s) & Y_{sq}(s) \\ Y_{ds}(s) & Y_{dd}(s) & Y_{dq}(s) \\ Y_{qs}(s) & Y_{qd}(s) & Y_{qq}(s) \end{bmatrix}}_{Y_{sdq}} \begin{bmatrix} \hat{V}_{dc}(s) \\ \hat{V}_d(s) \\ \hat{V}_q(s) \end{bmatrix} \quad (1)$$

The model reflects the relationship between the inputs: v_{dc} , v_d and v_q , and the outputs: i_{dc} , i_d and i_q .

2) *Measurement*: Experiments are conducted where time-domain step response data are collected and used along with the ERA toolbox to identify Y_{sdq} in s -domain [11]. In each experiment, a small-signal perturbation is injected to one of the input voltages and the resulted time-domain response data of all output currents are recorded. After that, all output data are fed to the ERA toolbox to identify their s -domain expressions. From there, $Y_{sdq}(s)$ can be found.

This paper focuses on investigating stability considering different dc-link control and power droop parameters. Fig. 3 and Fig. 4 show the obtained Bode plots of the measured 3×3 admittance considering different values of K and m compared to the original system, where m is the power droop coefficient ($m = 0.2$ in the base case), and K is associated with the dc-link controller gain ($K = 1$ in the base case).

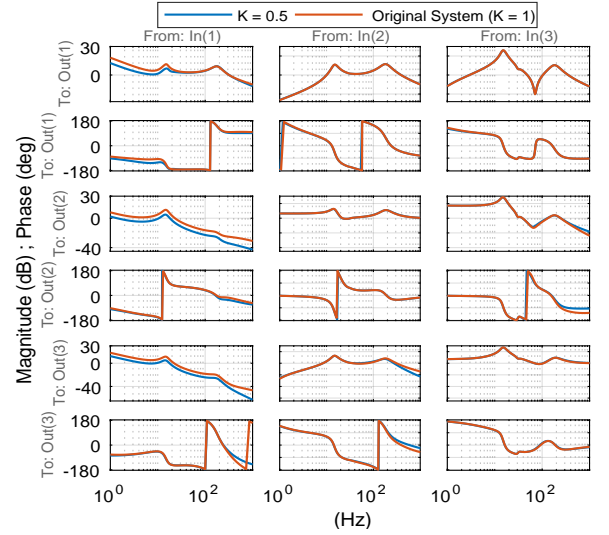


Fig. 3: Bode plots of the admittance for different values of dc-link controller gain (K).

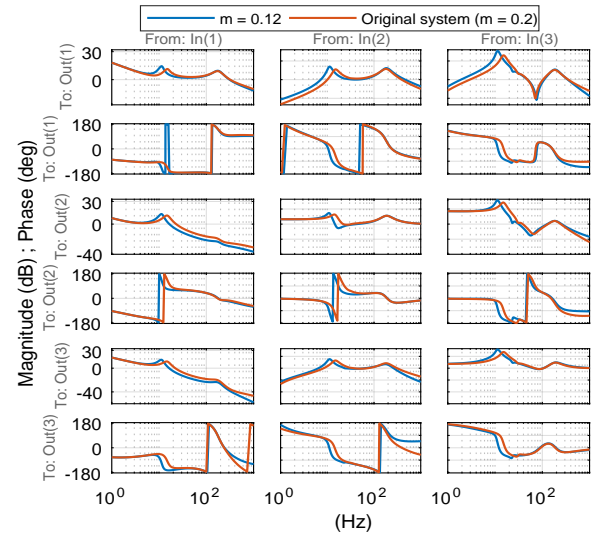


Fig. 4: Bode plots of the admittance for different values of power droop coefficient (m).

It can be seen that the dc-link controller gain influences the first column elements while the power droop coefficient

influences all 9 elements.

IV. STABILITY ANALYSIS

In order to analyze the effect of dc side network on the VSC system's stability, an admittance model including both the converter $Y_{sdq}(s)$ and the ac/dc side networks has to be developed. A brief derivation is given in the following paragraph.

The admittance model in (1) can be rearranged as shown in (2):

$$\begin{bmatrix} \hat{I}_{dc}(s) \\ \hat{I}_d(s) \\ \hat{I}_q(s) \end{bmatrix} = Y_{sdq} \begin{bmatrix} V_s \left(\frac{1}{RCs+1} \right) - I_{dc} \left(\frac{R}{RCs+1} \right) \\ \hat{V}_{gd}(s) \\ \hat{V}_{gq}(s) \end{bmatrix} - Z_{Line} \begin{bmatrix} \hat{I}_d(s) \\ \hat{I}_q(s) \end{bmatrix}. \quad (2)$$

The right side of (2) can be written as:

$$Y_{sdq} \begin{bmatrix} \left(\frac{1}{RCs+1} \right) & 0 & 0 \\ 0 & 1 & 0 \\ 0 & 0 & 1 \end{bmatrix} \begin{bmatrix} \hat{V}_s(s) \\ \hat{V}_{gd}(s) \\ \hat{V}_{gq}(s) \end{bmatrix} - Y_{sdq} \begin{bmatrix} \left(\frac{R}{RCs+1} \right) & 0 & 0 \\ 0 & Z_{Line_{dd}} & Z_{Line_{dq}} \\ 0 & Z_{Line_{qd}} & Z_{Line_{qq}} \end{bmatrix} \begin{bmatrix} \hat{I}_d(s) \\ \hat{I}_q(s) \end{bmatrix} \quad (3)$$

(2) leads to (4) & (5)

$$\underbrace{\left(\begin{bmatrix} 1 & 0 & 0 \\ 0 & 1 & 0 \\ 0 & 0 & 1 \end{bmatrix} + Y_{sdq} \begin{bmatrix} \left(\frac{R}{RCs+1} \right) & 0 & 0 \\ 0 & Z_{Line_{dd}} & Z_{Line_{dq}} \\ 0 & Z_{Line_{qd}} & Z_{Line_{qq}} \end{bmatrix} \right)}_C \begin{bmatrix} \hat{I}_{dc}(s) \\ \hat{I}_d(s) \\ \hat{I}_q(s) \end{bmatrix} = Y_{sdq} \underbrace{\begin{bmatrix} \left(\frac{1}{RCs+1} \right) & 0 & 0 \\ 0 & 1 & 0 \\ 0 & 0 & 1 \end{bmatrix}}_D \begin{bmatrix} \hat{V}_s(s) \\ \hat{V}_{gd}(s) \\ \hat{V}_{gq}(s) \end{bmatrix} \quad (4)$$

$$\begin{bmatrix} \hat{I}_{dc}(s) \\ \hat{I}_d(s) \\ \hat{I}_q(s) \end{bmatrix} = \underbrace{C^{-1} \cdot D}_{Y_{stability}} \begin{bmatrix} \hat{V}_s(s) \\ \hat{V}_{gd}(s) \\ \hat{V}_{gq}(s) \end{bmatrix} \quad (5)$$

Note that eigenvalues of the system are the zeros of $Y_{stability}(s)$.

A. Eigenvalue Analysis

1) *Original System* ($m = 0.2, K = 1$): Using the previously measured Y_{sdq} for the original system as shown in Fig. 3 or Fig. 4, $Y_{stability}(s)$ is then calculated for incremental values of R_{dc} . At each value, zeros of $Y_{stability}$ is found and plotted to have an eigenvalue loci trajectory showing the marginal condition. Fig. 5 shows eigenvalue loci for varying R_{dc} considering the original parameters of the VSC system. Results show that a 7-Hz mode is crossing the imaginary axis as R_{dc} reaches 1.48 pu.

2) *Effect of dc-link controller gain* (K): For reduced dc-link controller gain ($K = 0.5$), the zeros of $Y_{stability}$ at incremental values of R_{dc} are found and shown in Fig. 6. When R_{dc} reaches 1.25 pu, a 5-Hz mode reaches the imaginary axis.

3) *Effect of power droop coefficient* (m): For $m = 0.12$, zeros of $Y_{stability}$ at incremental values of R_{dc} are found and shown in Fig. 7. Noticeably, when the value of R_{dc} reaches 1.14 pu, a 7-Hz mode crosses the imaginary axis.

From the previous eigenvalue based analysis, it can be seen that decreasing the value of m or K reduces marginal stability.

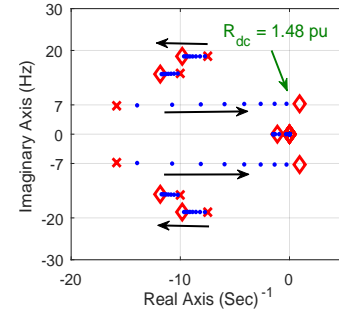


Fig. 5: Eigenvalue loci for varying R_{dc} in the original system ($m = 0.2, K = 1$).

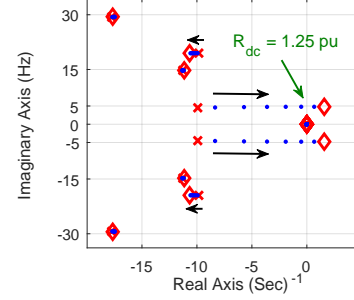


Fig. 6: Eigenvalue loci for varying R_{dc} in the VSC system where $K = 0.5$.

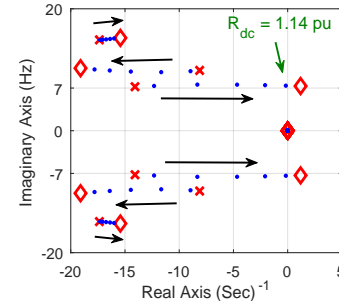


Fig. 7: Eigenvalue loci for varying R_{dc} in the VSC system where $m = 0.12$.

B. Open-loop Analysis

In the authors' prior work [11], it was shown how the scalar admittance viewed from the dc-side in (6) can be obtained via Kron reduction of the 3×3 admittance.

$$Y_{dc} = Y_{ss}(s) - \begin{bmatrix} Y_{sd}(s) & Y_{sq}(s) \end{bmatrix} Z_{Line} (Y_{dq} Z_{Line} + I)^{-1} \begin{bmatrix} Y_{ds}(s) \\ Y_{qs}(s) \end{bmatrix} \quad (6)$$

where

$$Z_{Line} = \begin{bmatrix} Z_{Line_{dd}} & Z_{Line_{dq}} \\ Z_{Line_{qd}} & Z_{Line_{qq}} \end{bmatrix}, Y_{dq} = \begin{bmatrix} Y_{dd}(s) & Y_{dq}(s) \\ Y_{qd}(s) & Y_{qq}(s) \end{bmatrix}, I = \begin{bmatrix} 1 & 0 \\ 0 & 1 \end{bmatrix}.$$

Therefore, using the previously measured admittance shown in Fig. 3, and Fig. 4, in addition to equation (6), the dc viewed admittance for different values of dc-link controller gain (K) and power droop coefficient (m) are found and shown in Fig. 6 and Fig. 7, respectively.

Now that Y_{dc} is found, and based on the dc side equivalent circuit shown in Fig. 10, the dc link voltage V_{dc} can be found

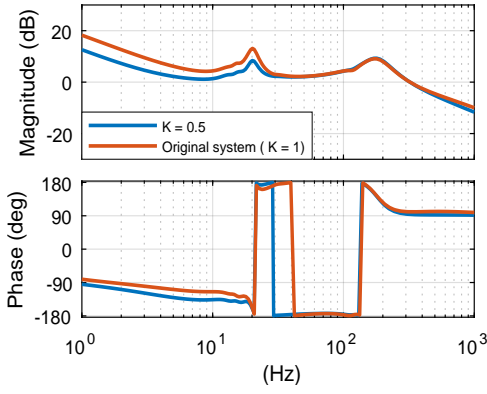


Fig. 8: dc viewed admittance for different values of dc-link controller gain (K).

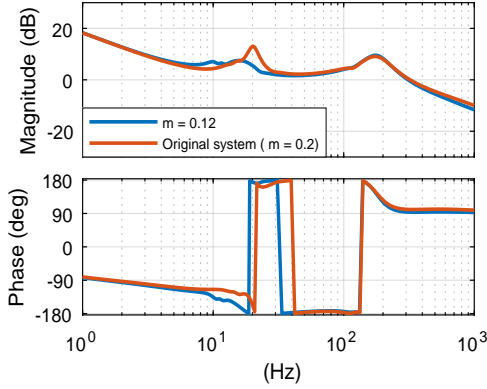


Fig. 9: Dc viewed admittance for different values of power droop coefficient (m).

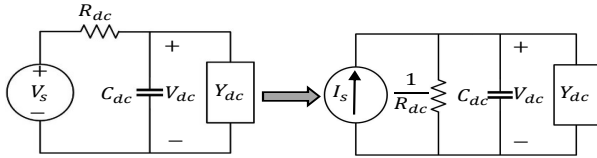


Fig. 10: Dc side equivalent circuit.

as:

$$V_{dc}(s) = \left(\frac{1}{Y_{dc}(s) + C_{dc}s + \frac{1}{R_{dc}}} \right) I_{inj}(s), \quad (7)$$

which can be rearranged to:

$$V_{dc}(s) = \left(\frac{1}{1 + R_{dc}(Y_{dc}(s) + C_{dc}s)} \right) R_{dc} \cdot I_{inj}(s) \quad (8)$$

From equation (8), the open-loop system can be seen clearly as

$$OL = R_{dc}(Y_{dc}(s) + C_{dc}s).$$

Therefore, the root-locus of $(Y_{dc}(s) + C_{dc}s)$ will show the closed-loop system pole trajectories as R_{dc} increases. The gain of the root loci reflects R_{dc} .

Fig. 11 presents the root loci for different values of dc-link controller gain (K) and power droop coefficient (m). The marginal gain (R_{dc}) when the dominant mode crosses the imaginary axis matches results obtained from the eigenvalue analysis.

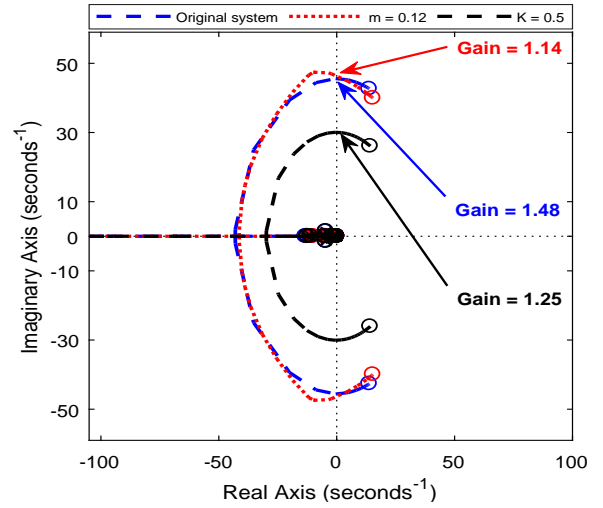


Fig. 11: Root loci for different values of (K), and (m) compared to original system.

C. Time-domain simulation results

The effects of R_{dc} , dc-link controller gain, and power droop coefficient on system stability are examined via EMT simulation. A small step change is applied in the ac voltage command to trigger dynamics.

1) *Effect of dc-link controller gain (K):* When R_{dc} reaches 1.252 pu, the dc-link voltage control at $K = 0.5$, shows oscillations, indicating marginal stability. For the original system where $K = 1$, at this condition, the system is stable. The time-domain responses of the two systems including both dc and ac sides are shown in Fig. 12. Around 4 \approx 5 Hz oscillations clearly appear in the dynamic response of the VSC system when $K = 0.5$.

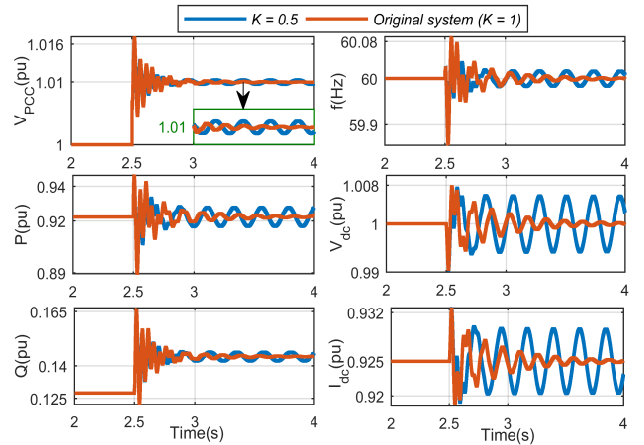


Fig. 12: Time-domain responses for a step change in the ac voltage command.

On the other hand, for the original VSC system ($K = 1$), when the value of R_{dc} reaches 1.488 pu, the dynamic responses of the system show oscillations after the dynamic trigger. Fig. 13 shows the original VSC system's response at $R_{dc} = 1.252$ pu, and $R_{dc} = 1.488$. Noticeably, ≈ 7 Hz oscillations appear when the value of R_{dc} is 1.488 pu. The EMT simulation results corroborate the analysis results.

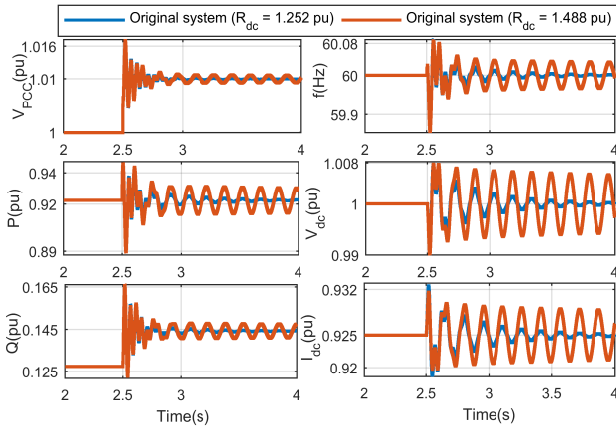


Fig. 13: Original VSC's responses after a step change in the ac voltage command.

2) *Effect of power droop coefficient (m):* When R_{dc} reaches 1.136 pu, the system (where $m = 0.12$) shows oscillations. For the original system (where $m = 0.2$), at this condition, it is stable. The dynamic responses of the two systems including dc and ac sides are shown in Fig. 14. ≈ 7 Hz oscillations clearly appear for $m = 0.12$.

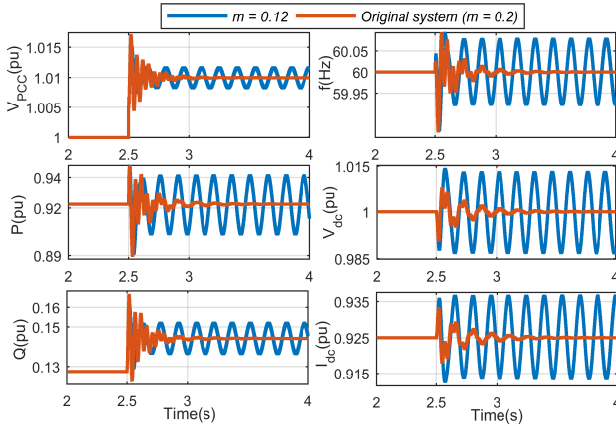


Fig. 14: Time-domain responses for a step change in ac voltage command.

For $m = 0.2$, it was found before that the maximum value of R_{dc} is 1.488 pu from the analysis. Fig. 15 shows the original VSC system's responses at $R_{dc} = 1.252$ pu, and $R_{dc} = 1.488$ pu. It can be clearly seen that the oscillations appear when R_{dc} is 1.488 pu.

Remarks: EMT simulation results corroborate the stability analysis results obtained from eigenvalue analysis based on the 3×3 admittance model and the SISO open-loop system viewed from the dc side.

V. CONCLUSION

In this paper, stability analysis of a grid-forming VSC system was performed using the 3×3 admittance model obtained from measurement data. The stability analysis results are verified by the time-domain simulation results. Effects of dc-link controller gain and power droop coefficient on stability are examined. Results show that both influence dc-network stability.

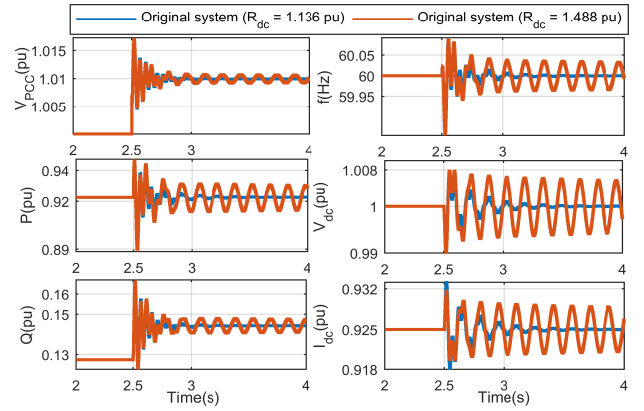


Fig. 15: Original VSC's responses after a step change in the ac voltage command.

REFERENCES

- [1] G. Denis, T. Prevost, M.-S. Debry, F. Xavier, X. Guillaud, and A. Menze, "The migrate project: the challenges of operating a transmission grid with only inverter-based generation. a grid-forming control improvement with transient current-limiting control," *IET Renewable Power Generation*, vol. 12, no. 5, pp. 523–529, 2018.
- [2] "U.s.energy information administration, independent statistics and analysis," accessed: 2021-09-30. [Online]. Available: <https://www.eia.gov/tools/faqs/faq.php?id=427&t=3>
- [3] H. Liu, X. Xie, J. He, T. Xu, Z. Yu, C. Wang, and C. Zhang, "Subsynchronous interaction between direct-drive pmsg based wind farms and weak ac networks," *IEEE Transactions on Power Systems*, vol. 32, no. 6, pp. 4708–4720, 2017.
- [4] S. H. Huang and G. Yanfeng, *South Texas SSR*. ERCOT ROS Meeting, May, 2018.
- [5] Joint NERC and WECC Staff, "900 mw fault induced solar photovoltaic resource interruption disturbance report southern california event: October 9, 2017," February 2018.
- [6] A. Yazdani and R. Iravani, *Voltage-sourced converters in power systems: modeling, control, and applications*. John Wiley & Sons, 2010.
- [7] X. Fu, J. Sun, M. Huang, Z. Tian, H. Yan, H. H.-C. Iu, P. Hu, and X. Zha, "Large-signal stability of grid-forming and grid-following controls in voltage source converter: a comparative study," *IEEE Transactions on Power Electronics*, vol. 36, no. 7, pp. 7832–7840, 2020.
- [8] W. Du, Z. Chen, K. P. Schneider, R. H. Lasseter, S. P. Nandanoori, F. K. Tuffner, and S. Kundu, "A comparative study of two widely used grid-forming droop controls on microgrid small-signal stability," *IEEE Journal of Emerging and Selected Topics in Power Electronics*, vol. 8, no. 2, pp. 963–975, 2019.
- [9] S. Almutairi, Z. Miao, and L. Fan, "Stability analysis of two types of grid-forming converters for weak grids," *International Transactions on Electrical Energy Systems*, p. e13136.
- [10] S. Shah and L. Parsa, "Impedance modeling of three-phase voltage source converters in dq, sequence, and phasor domains," *IEEE Transactions on Energy Conversion*, vol. 32, no. 3, pp. 1139–1150, 2017.
- [11] A. Aljumah, Z. Miao, and L. Fan, "Stability analysis of vsc systems using 3x3 admittance measurements," in *2021 IEEE Power & Energy Society General Meeting (PESGM)*, Accepted, 2021, pp. 1–5.
- [12] L. Zhang, L. Harnfors, and H.-P. Nee, "Power-synchronization control of grid-connected voltage-source converters," *IEEE Transactions on Power systems*, vol. 25, no. 2, pp. 809–820, 2009.